ELSEVIER

Physica E 13 (2002) 1155–1158

PHYSICA E

www.elsevier.com/locate/physe

Direct fabrication of parallel quantum dots with an atomic force microscope

U.F. Keyser[a,*], M. Paesler[a], U. Zeitler[a], R.J. Haug[a], K. Eberl[b]

[a] *Institut für Festkörperphysik, Universität Hannover, Appelstraße 2, 30167 Hannover, Germany*
[b] *Max-Plank-Institut für Festkörperforschung, Heisenbergstr. 1, 70569 Stuttgart, Germany*

Abstract

We demonstrate the stepwise fabrication of parallel double quantum dots in GaAs/AlGaAs-heterostructures. The atomic force microscope serves as a direct lithographic tool for the processing of our samples. The devices are characterized by transport measurements. Coulomb-blockade oscillations and diamonds with different periods for the two quantum dots are observed. © 2002 Elsevier Science B.V. All rights reserved.

PACS: ; 07.79.Lh; 85.40.Hp; 73.23.Hk; 73.23.b; 73.61.Ey

Keywords: Atomic force microscope; Double quantum dots; Transport measurements

Scanning probe microscopes allow the investigation of surfaces with sub-nm resolution. Since their development both the scanning tunneling microscope and the atomic force microscope (AFM) were used as tools for the modification of surfaces (for a review, see for e.g., Ref. [1]). The direct fabrication of electronic devices, quantum point contacts and single-electron transistors, in GaAs/AlGaAs-heterostructures using AFM-based techniques was demonstrated by several groups [2–6].

In this paper, we demonstrate the first stepwise fabrication of two parallel quantum dots with an AFM by performing current-controlled local anodic oxidation (LAO) and controlled nanomachining. The interesting feature of parallel quantum dots is the possible formation of coherent electronic states, see, e.g. [7]. Extensive studies on coupled dots were published by several groups [8], but these experiments were performed on devices with two quantum dots coupled in series or with only one dot connected to the leads [9]. With the conventional lithographic techniques, like electron-beam lithography, the definition of two quantum dots in parallel both connected to the same leads is a very challenging problem.

Our GaAs/AlGaAs-heterostructure was grown with molecular beam epitaxy. The layer sequence from top to bottom consists of a 10 nm thick GaAs cap layer, 15 nm Si-doped AlGaAs, 15 nm undoped AlGaAs spacer, and 500 nm of GaAs. A two-dimensional electron gas (2DEG) 40 nm below the surface is formed (carrier density 4×10^{15} m^{-2}, mobility 23 m^2/Vs). With optical lithography and wet-chemical etching Hall bars (width 10 μm) with eight contacts are defined and contacted with alloyed Au/Ge ohmic-contacts. After this processing, the samples are completely bonded and mounted into the AFM on a ceramic chip carrier.

* Corresponding author. Tel.: +49-(0)-511-762-19040; fax: +49-(0)-511-762-2904.
E-mail address: keyser@nano.uni-hannover.de (U.F. Keyser).

PII: S1386-9477(02)00325-9

During the first fabrication step the controlled nanomachining is done by applying a contact force of more than 10 μN and scanning the tip over the surface ($v_{tip} = 100$ μm/s). Grooves are scribed in the GaAs/AlGaAs to deplete the 2DEG underneath. The fabrication of the gates is controlled by in situ monitoring of the sample resistance. If the room-temperature resistance of a nanomachined line exceeds 3 MΩ, the tip is retracted. The low-temperature resistance of these lines is very high ($R > 50$ GΩ) over a wide voltage range (at least ±5 V). Therefore, it is possible to define gates for the control of the electrochemical potential of nanoscale devices. During this first step two in-plane gates (IPG) are nanomachined which define a lateral field effect transistor [10]. For more details on the fabrication process, see Ref. [5]. The width of the IPG-channel was chosen to be 2.7 μm for the device described in this paper. Taking into account the depletion length of approximately 350 nm around the nanomachined lines this leads to an active region of about 2.0 μm.

Following this processing, the IPG-transistor is tested at $T = 4.2$ K to check if the gates have the expected characteristic. Afterwards the sample is again mounted into the AFM.

During this second fabrication step, we add a double-barrier structure to the IPG-channel to define a lateral resonant tunneling diode (RTD). This is done using LAO. A conductive AFM-tip is negatively biased with respect to the grounded sample and scanned over the surface ($v_{tip} = 250$ nm/s). We are working with a relative humidity of 40–60% and use the naturally formed water film on the sample as electrolyte for the electrochemical oxidation of the sample. The tip is in contact with the surface and the oxidation current I_{ox} (typical 100 nA to 1 μA) is kept constant by varying the tip–sample voltage V_{t-s} (typical $|V_{t-s}| < 8$ V). The electronic height of the tunneling barriers depends linearly on I_{ox} [6].

The double-barrier structure is written across the IPG-channel with a distance of 250 nm between the tunneling barriers with an oxidation current $I_{ox} = 150$ nA. An AFM-image of the structure is shown in Fig. 1(a).

A sketch of the band structure parallel to the current direction I_{SD} is displayed in Fig. 1(b). The 1D-subband is coupled to the 2D-contacts by the two tunneling barriers, and can be tuned by the IPGs

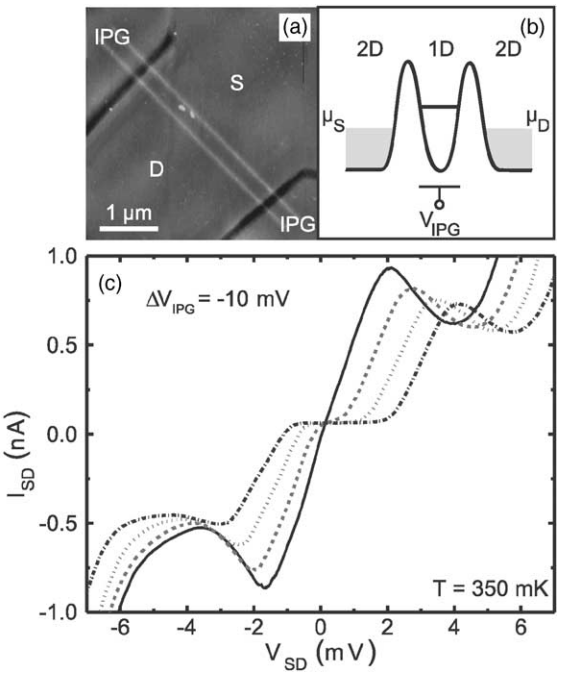

Fig. 1. (a) AFM-micrograph of a RTD. The IPG are defined by controlled nanomachining—the tunneling barriers (light gray) by current-controlled LAO. (b) Sketch of the conduction band of the RTD in (a). A 1D-subband is formed between the tunneling barriers and can be tuned by application of IPG-voltages. (c) Current traces at four different IPG-voltages (−650, −660, −670, −680 mV) in function of V_{SD} at $T = 350$ mK. The resonance is shifted and the peak-to-valley ratio is changed by the IPG-voltage.

relative to the electrochemical potentials of source μ_S and drain μ_D. Measurements of the device at $T = 350$ mK in a ^{3}He-system are presented in Fig. 1(c). Displayed is the current between source and drain I_{SD} in function of the voltage applied across the structure V_{SD}. The voltage of one IPG was stepped from −650 to −680 mV with $\Delta V_{IPG} = -10$ mV from top to bottom. All four curves show peaks in I_{SD} with negative differential conductance and a decreasing peak-to-valley ratio of 1.5 : 1 (−650 mV) to 1.1 : 1 (−680 mV). This demonstrates the tuneability of the position and shape of the resonance by an IPG-voltage which is interesting for possible applications. In earlier studies [11], we showed that this double-barrier structure encloses a quasi-1D-wire.

After this characterization step this device was again mounted into the AFM and another LAO-step was

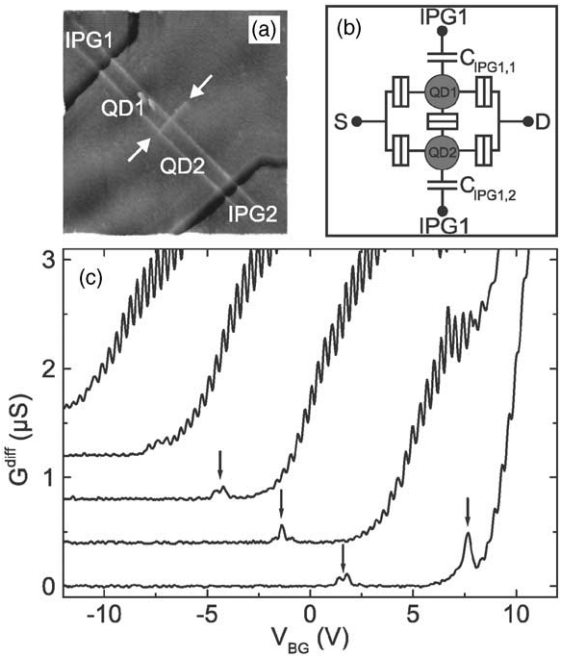

Fig. 2. (a) AFM-image of the parallel quantum dots, the RTD in Fig. 1(a) was cut. (b) Circuit diagram for one gate. Both QDs are controlled by one gate but with a different capacitance, e.g. $C_{IPG1,1}, C_{IPG1,2}$. (c) Measured differential conductance in function of backgate-voltage V_{BG} and stepwise variation of V_{IPG1} (from top to bottom: $-250\,mV \geqslant V_{IPG1} \geqslant -650\,mV$, $\Delta V_{IPG1} = -100\,mV$, $T = 350\,mK$). The curves are offset for clarity. At $V_{IPG1} = -250, -350\,mV$ Coulomb-blockade oscillations (CBO) of QD1 are observed (short period). For $V_{IPG1} \leqslant -450\,mV$ the CBOs of QD2 (marked with arrows) with a longer period appear.

done to cut the 1D-wire into two quantum dots labeled QD1 and QD2. In the AFM-micrograph (Fig. 2(a)), the sample is shown after performing the LAO. The tunneling barrier separating the dots was written with $I_{ox} = 300\,nA$ (compared to the double-barriers this should lead to lower tunnel coupling between QD1 and QD2 than to the contacts). A simple circuit diagram of the device is displayed in Fig. 2(b). Both dots share the same leads enabling parallel transport through them. For clarity, a configuration only with IPG1 is drawn. For the other gates (IPG2, backgate) one has to add two capacitances between each gate and QD1/QD2.

In Fig. 2(c), traces of the differential conductance $G^{diff} = dI_{SD}/dV_{SD}$ at $V_{SD} \approx 0.0\,mV$ in function of the backgate voltage V_{BG} were measured. The IPG2 was kept constant at $-100\,mV$ and IPG1 was stepped from -250 to $-650\,mV$ with $\Delta V = -100\,mV$. In the topmost curve ($V_{IPG1} = -250\,mV$), we observe Coulomb-blockade oscillations (CBO) with a capacitance of $C_{BG,1} \approx 0.4\,aF$ between the backgate and one quantum dot. We assign these fast oscillations to QD1. By lowering V_{IPG1} (lower curves) the onset of the QD1-oscillations is shifted to higher V_{BG} and at $V_{IPG1} = -450\,mV$ a new peak appears (marked with an arrow). Finally at $-650\,mV$, we observe the second CBO with a lower period and attribute it to QD2 with a capacitance of $C_{BG,2} \approx 0.03\,aF$ to the backgate. At lower negative voltage on V_{IPG1}, the conductance of the device is dominated by QD1, at higher negative V_{IPG1} we measure both the CBOs of QD1 and QD2. Thus, with IPG1 we can control the current flow through the two quantum dots. From the AFM micrograph one would expect that both dots should have the same size. But our results from above indicate that QD2 is smaller than QD1. One possible explanation is a wider depleted region around the groove defining IPG2 which is 3 nm deeper than the groove of IPG1.

Since the distance between dot and gate should determine the capacitance, we extracted the capacitances from the measurements. The capacitance between QD1 and IPG1 $C_{IPG1,1} \approx 10\,aF$ is calculated from the shift of the CBO of QD1 by applying $\Delta V_{IPG1} = -100\,mV$ in Fig. 2(c) with $C_{IPG1,1} = \Delta C_{BG}/\Delta C_{IPG1} \times C_{BG,1}$. For the capacitance between IPG1 and QD2, we get $C_{IPG1,2} \approx 0.9\,aF$. The capacitances $C_{IPG2,1} \approx 8\,aF$ and $C_{IPG2,2} \approx 1.1\,aF$ were determined by similar measurements to that in Fig. 2(a), but stepping V_{IPG2} and $V_{IPG1} = const$. From the AFM-image in Fig. 2(a), we would expect that $C_{IPG1,1} \approx C_{IPG2,2}$ but, as stated above, QD2 is smaller than QD1 and thus we get $C_{IPG1,1} > C_{IPG2,2}$. With the above values, we get $C_{IPG1,1} > C_{IPG2,1}$ and $C_{IPG1,2} < C_{IPG2,2}$ which is an indication that the distance between QD1 and IPG1 is smaller than between QD1 and IPG2 and vice versa for QD2.

To obtain the overall capacitances of the QDs in Fig. 3 a grayscale-plot of the absolute value of the source–drain current I_{SD} of the device in Fig. 2(a) is shown. The backgate-voltage V_{BG} and the source–drain voltage V_{SD} were swept—the IPGs were constantly biased with $-550\,mV$ (IPG1) and $-330\,mV$ (IPG2). To observe the signature of both dots, we shift the onset of QD1 to higher V_{BG} by applying $V_{IPG1} = -550\,mV$. We can identify Coulomb-blockade

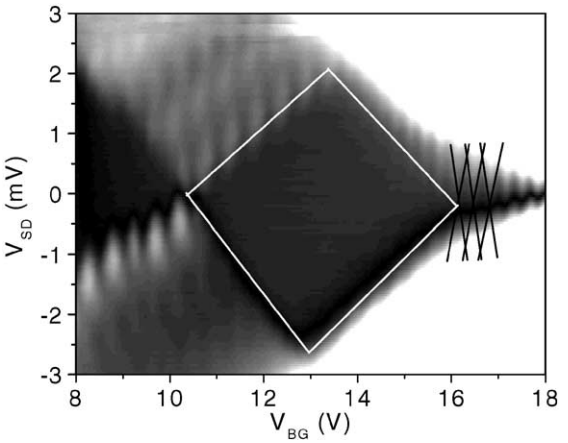

Fig. 3. Absolute value of the current I_{SD} through the double-dot as function of backgate V_{BG} and source–drain voltage V_{SD} (black: $I_{SD} = 0.0$ nA, white: $I_{SD} > 100$ pA–$V_{IPG1} = -550$ mV, $V_{IPG2} = -300$ mV). At $V_{BG} < 16$ V, the transport is dominated by QD2 (large coulomb-blockade diamond, indicated by white line) at $V_{BG} > 16$ V the current flows through QD1 (small diamonds, black lines).

diamonds with two different sizes for QD1 and QD2. At high backgate-voltage ($V_{BG} > 16$ V), we observe many small diamonds—some are indicated with black lines. By analyzing the maximal width $V_{SD,max}$, we obtain the overall capacitance C_Σ of QD1 with $2e^2/C_\Sigma = eV_{SD,max}$ to be $C_{\Sigma,1} \approx 250 \pm 10$ aF. Indicated by the white lines is a large diamond at $V_{BG} < 16$ V which we can attribute to the QD2 with $C_{\Sigma,2} \approx 70 \pm 15$ aF. The capacitances differ by a factor of four, this is another indication that QD2 is considerably smaller than QD1.

In conclusion, we have demonstrated the first stepwise fabrication of a parallel double quantum-dot with controlled nanomachining and current-controlled local anodic oxidation. The dot was defined by splitting a quasi-one-dimensional resonant tunneling diode (RTD) in two seperate regions. Consecutive transport measurements on the device showed the typical negative differential conductance for the RTD and Coulomb-blockade oscillations and diamonds for the two quantum dots.

References

[1] C.R.K. Marrian (Ed.), Special Issue on Nanometer-Scale Science and Technology, Proceedings of the IEEE, Vol. 85, 1997, pp. 481–704.
[2] M. Ishii, K. Matsumoto, Jpn. J. Appl. Phys. 34 (1995) 1329.
[3] R. Held, et al., Appl. Phys. Lett. 73 (1998) 262; S. Luscher, et al., Phys. Rev. Lett. 86 (2001) 2118.
[4] N.J. Curson, et al., Appl. Phys. Lett. 78 (2001) 3466.
[5] H.W. Schumacher, et al., Appl. Phys. Lett. 75 (1999) 11070; H.W. Schumacher, et al., Physica E 9 (2000) 860.
[6] U.F. Keyser, et al., Appl. Phys. Lett. 76 (2000) 457.
[7] L.P. Kouwenhoven, et al., in: L.L. Sohn, L.P. Kouwenhoven, G. Schön (Eds.), Mesoscopic Electron Transport, Proceedings of a NATO Advanced Study Institute, Kluwer, Dordrecht, 1997.
[8] C. Livermore, et al., Science 274 (1996) 1332; R.H. Blick, et al., Phys. Rev. B 53 (1996) 7899; R.H. Blick, et al., Phys. Rev. Lett. 80 (1998) 4032; T.H. Oosterkamp, et al., Nature 395 (1998) 873.
[9] F. Hofmann, et al., Phys. Rev. B 51 (1995) 13872.
[10] A.D. Wieck, K. Ploog, Appl. Phys. Lett. 56 (1990) 928.
[11] U.F. Keyser, et al., Phys. Stat. Sol. 224 (2001) 685.